



HAL
open science

Hierarchical modeling of heterogeneous solids

J. Tinsley Oden, Kumar Vemaganti, Nicolas Moës

► **To cite this version:**

J. Tinsley Oden, Kumar Vemaganti, Nicolas Moës. Hierarchical modeling of heterogeneous solids. *Computer Methods in Applied Mechanics and Engineering*, 1999, 172 (1-4), pp.3-25. 10.1016/S0045-7825(98)00224-2 . hal-04243925

HAL Id: hal-04243925

<https://hal.science/hal-04243925>

Submitted on 29 Oct 2023

HAL is a multi-disciplinary open access archive for the deposit and dissemination of scientific research documents, whether they are published or not. The documents may come from teaching and research institutions in France or abroad, or from public or private research centers.

L'archive ouverte pluridisciplinaire **HAL**, est destinée au dépôt et à la diffusion de documents scientifiques de niveau recherche, publiés ou non, émanant des établissements d'enseignement et de recherche français ou étrangers, des laboratoires publics ou privés.

Hierarchical modeling of heterogeneous solids

J. Tinsley Oden*, Kumar Vemaganti, Nicolas Moës

Texas Institute for Computational and Applied Mathematics, The University of Texas at Austin, Austin, TX 78712, USA

Abstract

The modeling of microscale effects required to describe physical phenomena such as the deformation of highly heterogeneous materials makes the use of standard simulation techniques prohibitively expensive. Most homogenization techniques that have been proposed to circumvent this problem lose small-scale information and as a result tend to produce acceptable results only for narrow classes of problems.

The concept of *hierarchical modeling* has been advanced as an approach to overcome the difficulties of multiscale modeling. Hierarchical modeling can be described as the methodology underlying the adaptive selection of mathematical models from a well-defined class of models so as to deliver results of a preset level of accuracy. Thus, it provides a framework for the automatic and adaptive selection of the most essential scales involved in a simulation.

In the present paper, we review the Homogenized Dirichlet Projection Method (HDPM) [J.T. Oden and T.I. Zohdi, *Comput. Methods Appl. Mech. Engrg.* 148 (1997) 367–391; T.I. Zohdi, J.T. Oden and G.J. Rodin, *Comput. Methods Appl. Mech. Engrg.* 138 (1996) 273–298] and present several extensions of its underlying theory. We present global energy-norm and L^2 estimates of the modeling error resulting from homogenization. In addition, new theorems and methods for estimating error in local quantities of interest, such as mollifications of local stresses are presented. These a posteriori estimates form the basis of the HDPM. Finally, we extend the HDPM to models of local failure and damage of two-phase composite materials. The results of several numerical experiments and applications are given.

1. Introduction

The ability to analyze and accurately model heterogeneous and composite materials has assumed greater importance as the need to account for micromechanical effects in predicting the service life of machine parts and structures is more broadly accepted. One of the main features of these materials is that their response to loads and forces is often a complex multiscale, multiphysics phenomenon. Despite advances in computational techniques and computing power, direct simulation of heterogeneous materials is still not a viable option. Finite element models that can capture micromechanical effects generally must employ mesh sizes of the order of the size of the microstructure and can result in an algebraic system with many millions of unknowns. On the other hand, homogenization and averaging techniques for analyzing heterogeneous materials, while possibly leading to manageable problem sizes, do not provide information about the microscopic fields needed, for example, to predict failure. Thus there is a need for accurate and computationally efficient techniques that take into account the most important scales involved in the goal of the simulation while permitting the analyst to choose the level of accuracy and detail of description desired.

Towards this end, the concept of hierarchical modeling was introduced [13,9] as a methodology that provides a multilevel description of the physical phenomenon of interest based, when possible, on a rigorous mathematical foundation. A hierarchy of descriptions of the physics of the problem is first set up, ranging from

* Corresponding author.

the coarsest possible description to the most detailed description contained in the class of models. Rather than to heuristically choose a level of description from the hierarchy, a posteriori estimates of the modeling error associated with a particular description are evaluated to enable the adaptive selection of a suitable characterization. Also, the level of description is allowed to vary spatially so that finer descriptions may be used in ‘critical’ regions.

Based on this concept of hierarchical modeling, the Homogenized Dirichlet Projection Method (HDPM) was developed in [13,9]. In this method, at the coarsest level in the hierarchy of models is a mathematical model characterized by homogenized material properties. This is referred to as the homogenized problem and the lack of heterogeneity generally makes this problem computationally inexpensive compared to models of finer scale. The adequacy of the solution to this homogenized problem, compared to the fine-scale solution, is then estimated using a posteriori modeling error estimates. In regions where the modeling error exceeds a preset tolerance, a finer-scale model is used and a correction to the homogenized solution is computed. This process is continued until a simulation is obtained which is sufficiently accurate to satisfy preset error tolerances. Fuller details of this procedure are given later in this investigation.

While the use of hierarchical modeling permits the adaptive reduction of modeling error, it is equally important to control the numerical error associated with the approximation of each model used in the analysis. In our computations in this work, we employ an adaptive 3-d *hp* finite element method to control and minimize the effect of numerical error on our results. The use of *hp* finite elements significantly enhances the quality of the final solution obtained with HDPM while reducing the number of DOF required to solve both local and global problems.

The use of hierarchical modeling presents some intriguing observations on modeling of structures. The final computational model achieved by, say, the HDPM to meet a given tolerance, may exhibit highly nonuniform material characterizations that depend upon the data in the simulations (the geometry, loads, boundary conditions, etc.) and the norms used to control the error. Thus, different tolerances and different norms lead to different material characterizations. We present here new error estimation results for control of L^2 error and error in local quantities of interest.

We also describe the extensions of the HDPM to a class of nonlinear problems involving local damage and possible crack initiation. We describe an application of HDPM to a two-phase composite in which local failure is assumed to occur when the local stresses reach a prescribed limit value. When this limit is attained, the local stiffness in a neighborhood of the failure point vanishes and a local redistribution of stresses takes place. Cycles of HDPM for the damaged structure are repeated until the damage is arrested or full failure occurs.

The outline of the presentation in this paper is as follows. We first present some preliminaries and notation and set up the model class of problems under consideration. In Section 3, we present energy and L^2 estimates of the error associated with the homogenized solution. In Section 4, we briefly describe the HDPM. Next, in Section 5, we develop an estimate of the homogenization error in quantities of interest described by linear functionals on the space of admissible displacements. This is followed by numerical examples in Section 6. In the numerical applications, we describe a straightforward extension of the HDPM to problems of local damage and of simulating accumulative damage in a two-phase composite. Finally, we offer some comments and discuss future directions of research in this area.

2. Preliminaries

In this section we describe the notation and conventions to be adopted in our analysis. The model problem characterizing the exact or fine-scale problem and the homogenized problem are presented followed by an analysis of the error introduced by homogenization.

2.1. Notation and the exact problem

We consider the familiar problem of linear elastostatics describing the deformation of a heterogeneous body in static equilibrium under the action of body forces \mathbf{f} and boundary tractions \mathbf{t} . The body occupies an open bounded domain $\Omega \subset \mathbb{R}^N$, $N = 1, 2, 3$. The boundary $\partial\Omega$ of the body is assumed to be Lipschitz and consists of

a portion Γ_u on which displacements are prescribed and a part Γ_t on which tractions are prescribed and $\partial\Omega = \Gamma_u \cup \Gamma_t$, $\Gamma_u \cap \Gamma_t = \emptyset$.

Vector and tensor valued functions defined over Ω are denoted by boldface letters and repeated indices indicate summation. As usual, $H^1(\Omega)$ stands for the space of scalar valued functions with distributional derivatives of order ≤ 1 in $L^2(\Omega)$. We also define $\mathbf{H}^1(\Omega) \stackrel{\text{def}}{=} (H^1(\Omega))^N$ as the space of vector valued functions whose components are all in $H^1(\Omega)$ and similarly we denote $\mathbf{L}^2(\Omega) \stackrel{\text{def}}{=} (L^2(\Omega))^N$. The spaces $\mathbf{H}^1(\Omega)$ and $\mathbf{H}^1(\Omega)$ are equipped with the norms

$$\|\mathbf{v}\|_{\mathbf{H}^1(\Omega)}^2 \stackrel{\text{def}}{=} \sum_{i=1}^N \|v_i\|_{H^1(\Omega)}^2, \quad \|\mathbf{v}_i\|_{H^1(\Omega)}^2 \stackrel{\text{def}}{=} \int_{\Omega} \sum_{|\alpha| \leq 1} |D^\alpha v_i|^2 dx \quad (1)$$

respectively, where v_i are the cartesian components of \mathbf{v} . Values of functions $\mathbf{v} \in \mathbf{H}^1(\Omega)$ on Γ_u are understood in the sense of traces and denoted $\mathbf{v}|_{\Gamma_u}$. It is also assumed that the loading is such that $\mathbf{f} \in \mathbf{L}^2(\Omega)$ and $\mathbf{t} \in \mathbf{L}^2(\Gamma_t)$. Next, the body is assumed to be characterized by an elasticity tensor \mathbf{E} which is a bounded function in $\mathbb{R}^{N^2 \times N^2}$ and satisfies the following conditions of ellipticity and symmetry: $\exists \alpha_i, \alpha_u > 0$ such that $\forall \mathbf{A} \in \mathbb{R}^{N \times N}$, $\mathbf{A} = \mathbf{A}^T$,

$$\begin{aligned} \alpha_i \mathbf{A} : \mathbf{A} &\leq \mathbf{A} : \mathbf{E}(\mathbf{x}) \mathbf{A} \leq \alpha_u \mathbf{A} : \mathbf{A}, \quad \mathbf{x} \in \Omega \\ E_{ijkl}(\mathbf{x}) &= E_{jikl}(\mathbf{x}) = E_{ijlk}(\mathbf{x}) = E_{klij}(\mathbf{x}) \quad 1 \leq i, j, k, l \leq N, \end{aligned} \quad (2)$$

$E_{ijkl}(\mathbf{x})$ being the cartesian components of the elasticity tensor \mathbf{E} . The ellipticity condition states that the strain energy of the body is positively finite for admissible non-zero strain fields; the symmetry condition restricts the number of independent components in the elasticity tensor.

The displacement boundary conditions on Γ_u are specified as follows: $\exists \hat{\mathbf{u}} \in \mathbf{H}^1(\Omega)$ such that $\hat{\mathbf{u}}|_{\Gamma_u} = \mathcal{U}$, where \mathcal{U} is the prescribed displacement data on Γ_u . Then the principle of virtual work governing the displacement field in the body leads to the following problem:

Find $\mathbf{u} \in \{\hat{\mathbf{u}}\} + V(\Omega)$ such that

$$\mathcal{B}(\mathbf{u}, \mathbf{v}) = \mathcal{F}(\mathbf{v}) \quad \forall \mathbf{v} \in V(\Omega),$$

(3)

where the space of admissible functions $V(\Omega)$ is defined as

$$V(\Omega) \stackrel{\text{def}}{=} \{\mathbf{v} : \mathbf{v} \in \mathbf{H}^1(\Omega), \mathbf{v}|_{\Gamma_u} = \mathbf{0}\}. \quad (4)$$

The bilinear and linear forms are defined as

$$\mathcal{B}(\mathbf{u}, \mathbf{v}) \stackrel{\text{def}}{=} \int_{\Omega} \nabla \mathbf{v} : \mathbf{E} \nabla \mathbf{u} dx = \int_{\Omega} \text{tr}[(\nabla \mathbf{v})^T \mathbf{E} \nabla \mathbf{u}] dx \quad (5)$$

and

$$\mathcal{F}(\mathbf{v}) \stackrel{\text{def}}{=} \int_{\Omega} \mathbf{f} \cdot \mathbf{v} dx + \int_{\Gamma_t} \mathbf{t} \cdot \mathbf{v} ds. \quad (6)$$

If the solution to (3) and the data are sufficiently regular, which is rarely the case, then it satisfies the following equations of classical elasticity,

$$\begin{aligned} -\nabla \cdot \mathbf{E}(\mathbf{x}) \nabla \mathbf{u}(\mathbf{x}) &= \mathbf{f}(\mathbf{x}) & \mathbf{x} \in \Omega \\ \mathbf{u}(\mathbf{x}) &= \mathcal{U}(\mathbf{x}) & \mathbf{x} \in \Gamma_u \\ \mathbf{n} \cdot (\mathbf{E}(\mathbf{x}) \nabla \mathbf{u}(\mathbf{x})) &= \mathbf{t}(\mathbf{x}) & \mathbf{x} \in \Gamma_t. \end{aligned}$$

(7)

2.2. The homogenized problem

For the type of problems considered in this paper, \mathbf{E} is a highly oscillatory function thus making the use of conventional methods like finite elements computationally expensive and in most cases, impossible. This problem can however be made more amenable to computation through standard homogenization processes whereby \mathbf{E} is replaced by a function \mathbf{E}^0 , often a constant, that is designed to characterize the macroscopic behavior of the structure. The loading due to body force and tractions is assumed to remain unchanged, but this assumption could also be relaxed without significantly complicating our analysis.

The homogenized elasticity tensor is also assumed to satisfy ellipticity and symmetry conditions similar to (2) with ellipticity constants β_l and β_u , i.e. $\exists \beta_l, \beta_u > 0$ such that $\forall \mathbf{A} \in \mathbb{R}^{N \times N}, \mathbf{A} = \mathbf{A}^T$,

$$\begin{aligned} \beta_l \mathbf{A} : \mathbf{A} &\leq \mathbf{A} : \mathbf{E}^\bullet(x) \mathbf{A} \leq \beta_u \mathbf{A} : \mathbf{A} \\ E_{ijkl}^0(x) &= E_{jikl}^0(x) = E_{ijlk}^0(x) = E_{klij}^0(x) \quad 1 \leq i, j, k, l \leq N. \end{aligned} \quad (8)$$

The homogenized problem thus reads

$$\boxed{\begin{aligned} \text{Find } \mathbf{u}^0 \in \{\hat{\mathbf{u}}\} + \mathbf{V}(\Omega) \text{ such that} \\ \mathcal{B}^0(\mathbf{u}^0, \mathbf{v}) = \mathcal{F}(\mathbf{v}) \quad \forall \mathbf{v} \in \mathbf{V}(\Omega) \end{aligned}} \quad (9)$$

with

$$\mathcal{B}^0(\mathbf{u}^0, \mathbf{v}) \stackrel{\text{def}}{=} \int_{\Omega} \nabla \mathbf{v} : \mathbf{E}^0 \nabla \mathbf{u}^0 \, dx \quad (10)$$

and with the right-hand side as defined earlier. Again, if the solution to the homogenized problem represented by (9) is sufficiently regular, then it also satisfies the following homogenized equations,

$$\boxed{\begin{aligned} -\nabla \cdot \mathbf{E}^\bullet(x) \nabla \mathbf{u}^0(x) &= \mathbf{f}(x) & x \in \Omega \\ \mathbf{u}^0(x) &= \mathcal{U}(x) & x \in \Gamma_u \\ \mathbf{n} \cdot (\mathbf{E}^0(x) \nabla \mathbf{u}^0(x)) &= \mathbf{t}(x) & x \in \Gamma_t. \end{aligned}} \quad (11)$$

3. Analysis of the homogenization error

The homogenized solution \mathbf{u}^\bullet is obviously in error because material information is lost due to the process of homogenization. The homogenization or modeling error is defined as the difference between the exact solution and the homogenized solution, $\mathbf{e}^0 \stackrel{\text{def}}{=} \mathbf{u} - \mathbf{u}^0$.

To be able to develop adaptive methods of simulation, it is important to evaluate the quality of the homogenized solution. In this section, we present various measures of the homogenization error \mathbf{e}^0 as well as a measure of the error in the stresses between the exact and homogenized solutions.

3.1. An energy estimate of the homogenization error

The following theorem is proved in [13].

THEOREM 3.1. *Let \mathbf{u} and \mathbf{u}^0 be the solutions to problems (3) and (9), respectively. Then, the following holds:*

$$\|\mathbf{e}^\bullet\|_{E(\Omega)}^2 = \|\mathbf{u} - \mathbf{u}^0\|_{E(\Omega)}^2 \leq \zeta^2 \stackrel{\text{def}}{=} \int_{\Omega} \mathcal{I}_0 \nabla \mathbf{u}^0 : \mathbf{E} \mathcal{I}_0 \nabla \mathbf{u}^0 \, dx \quad (12)$$

where

$$\mathcal{J}_0 \stackrel{\text{def}}{=} (\mathbf{I} - \mathbf{E}^{-1} \mathbf{E}^0) \quad (13)$$

□

Thus, if the solution to (9) is known, the homogenization error is bounded by a quantity that can be expressed in terms of known quantities.

3.2. An L^2 estimate of the homogenization error

Another global estimate of the homogenization error is presented below.

THEOREM 3.2. *Let \mathbf{u} and \mathbf{u}^0 be as above. Then, the following estimate holds*

$$\|\mathbf{e}^0\|_{L^2(\Omega)} = \|\mathbf{u} - \mathbf{u}^0\|_{L^2(\Omega)} \leq \frac{C(\Omega)}{\alpha_t} \|\mathbf{E} \mathcal{J}_0 \nabla \mathbf{u}^0\|_{L^2(\Omega)} \quad (14)$$

where α_t is defined in (2) and $C(\Omega)$ is a positive constant depending on the domain Ω .

PROOF. It can be easily verified that the homogenization error \mathbf{e}^\bullet is the solution to the following problem:

Find $\mathbf{e}^\bullet \in \mathbf{V}(\Omega)$ such that $\mathcal{B}(\mathbf{e}^\bullet, \mathbf{v}) = \mathcal{R}^\bullet(\mathbf{v}) \quad \forall \mathbf{v} \in \mathbf{V}(\Omega)$	(15)
---	------

where the right-hand side is defined as

$$\mathcal{R}^\bullet(\mathbf{v}) = - \int_{\Omega} \nabla \mathbf{v} : \mathbf{E} \mathcal{J}_0 \nabla \mathbf{u}^\bullet \, dx. \quad (16)$$

Setting $\mathbf{v} = \mathbf{e}^\bullet$, we have

$$\mathcal{B}(\mathbf{e}^\bullet, \mathbf{e}^\bullet) = \int_{\Omega} \nabla \mathbf{e}^\bullet : \mathbf{E} \nabla \mathbf{e}^\bullet \, dx = - \int_{\Omega} \nabla \mathbf{e}^\bullet : \mathbf{E} \mathcal{J}_0 \nabla \mathbf{u}^\bullet \, dx \quad (17)$$

The left-hand side of (17) can be bounded below,

$$\int_{\Omega} \nabla \mathbf{e}^\bullet : \mathbf{E} \nabla \mathbf{e}^\bullet \, dx \geq \alpha_t \int_{\Omega} \nabla \mathbf{e}^\bullet : \nabla \mathbf{e}^\bullet \, dx = \alpha_t \|\nabla \mathbf{e}^\bullet\|_{L^2(\Omega)}^2 \quad (18)$$

and the right-hand side can be bounded above using the Cauchy–Schwartz inequality,

$$- \int_{\Omega} \nabla \mathbf{e}^\bullet : \mathbf{E} \mathcal{J}_0 \nabla \mathbf{u}^\bullet \, dx \leq \|\nabla \mathbf{e}^\bullet\|_{L^2(\Omega)} \|\mathbf{E} \mathcal{J}_0 \nabla \mathbf{u}^\bullet\|_{L^2(\Omega)} \quad (19)$$

thus leading to

$$\|\nabla \mathbf{e}^\bullet\|_{L^2(\Omega)} \leq \frac{1}{\alpha_t} \|\mathbf{E} \mathcal{J}_0 \nabla \mathbf{u}^\bullet\|_{L^2(\Omega)}. \quad (20)$$

Now, we use the *Poincaré* inequality

$$\|\mathbf{v}\|_{L^2(\Omega)} \leq C(\Omega) \|\nabla \mathbf{v}\|_{L^2(\Omega)} \quad \forall \mathbf{v} \in \mathbf{V}(\Omega) \quad (21)$$

with (20) and the assertion follows. □

3.3. An estimate of the error in the stresses

The final estimate presented in this section provides an upper bound on the error in the stresses corresponding to the exact and the homogenized solutions.

THEOREM 3.3. *Let \mathbf{u} and \mathbf{u}^0 be as above. Define the stress states associated with these solutions as follows:*

$$\boldsymbol{\sigma} = \mathbf{E}\nabla\mathbf{u}, \quad \boldsymbol{\sigma}_0 = \mathbf{E}^0\nabla\mathbf{u}^0 \quad (22)$$

Then,

$$\|\boldsymbol{\sigma} - \boldsymbol{\sigma}_0\|_{L^2(\Omega)} \leq 2\sqrt{\alpha_u}\zeta \quad (23)$$

where α_u is defined in (2).

PROOF. First, we decompose the difference between $\boldsymbol{\sigma}$ and $\boldsymbol{\sigma}_0$,

$$\begin{aligned} \boldsymbol{\sigma} - \boldsymbol{\sigma}_0 &= \mathbf{E}\nabla\mathbf{u} - \mathbf{E}^0\nabla\mathbf{u}^0 + \mathbf{E}\nabla\mathbf{u}^0 - \mathbf{E}\nabla\mathbf{u}^0 \\ &= \mathbf{E}\nabla\mathbf{e}^0 + \mathbf{E}\mathcal{J}_0\nabla\mathbf{u}^0. \end{aligned} \quad (24)$$

Using the triangle inequality,

$$\|\boldsymbol{\sigma} - \boldsymbol{\sigma}_0\|_{L^2(\Omega)} \leq \|\mathbf{E}\nabla\mathbf{e}^0\|_{L^2(\Omega)} + \|\mathbf{E}\mathcal{J}_0\nabla\mathbf{u}^0\|_{L^2(\Omega)}. \quad (25)$$

The first term on the right-hand side of (25) can be bounded above, since under the assumptions in place \mathbf{E} has a well-defined square root.

$$\begin{aligned} \|\mathbf{E}\nabla\mathbf{e}^0\|_{L^2(\Omega)}^2 &= \int_{\Omega} \mathbf{E}\nabla\mathbf{e}^0 : \mathbf{E}\nabla\mathbf{e}^0 \, dx \\ &= \int_{\Omega} (\sqrt{\mathbf{E}}\nabla\mathbf{e}^0) : \mathbf{E}(\sqrt{\mathbf{E}}\nabla\mathbf{e}^0) \, dx \\ &\leq \alpha_u \int_{\Omega} (\sqrt{\mathbf{E}}\nabla\mathbf{e}^0) : (\sqrt{\mathbf{E}}\nabla\mathbf{e}^0) \, dx \\ &\leq \alpha_u \int_{\Omega} \nabla\mathbf{e}^0 : \mathbf{E}\nabla\mathbf{e}^0 \, dx \\ &\leq \alpha_u \|\mathbf{e}^0\|_{E(\Omega)}^2 \\ &\leq \alpha_u \zeta^2 \end{aligned} \quad (26)$$

thus leading to

$$\|\mathbf{E}\nabla\mathbf{e}^0\|_{L^2(\Omega)} \leq \sqrt{\alpha_u}\zeta. \quad (27)$$

The second term on the right-hand side of (25) can also be bounded similarly:

$$\begin{aligned} \|\mathbf{E}\mathcal{J}_0\nabla\mathbf{u}^0\|_{L^2(\Omega)}^2 &= \int_{\Omega} \mathbf{E}\mathcal{J}_0\nabla\mathbf{u}^0 : \mathbf{E}\mathcal{J}_0\nabla\mathbf{u}^0 \, dx \\ &\leq \alpha_u \int_{\Omega} \mathcal{J}_0\nabla\mathbf{u}^0 : \mathbf{E}\mathcal{J}_0\nabla\mathbf{u}^0 \, dx \\ &\leq \alpha_u \zeta^2 \\ \Rightarrow \|\mathbf{E}\mathcal{J}_0\nabla\mathbf{u}^0\|_{L^2(\Omega)} &\leq \sqrt{\alpha_u}\zeta \end{aligned} \quad (28)$$

Finally, combining (25), (27) and (28), the assertion follows. \square

We present other a posteriori estimates of modeling error in Section 5.

4. The Homogenized Dirichlet Projection Method (HDPM)

The HDPM is discussed in detail in [9,12,13]. The role of numerical error in HDPM is discussed in [8]. In this section, we summarize the major aspects of this method. We begin by noting that the homogenized solution \mathbf{u}^0 can in general be a poor approximation to the fine-scale solution \mathbf{u} . The error in the homogenized solution

depends mainly on the homogenized material properties. Typically, most homogenization techniques provide satisfactory solutions when the microstructure is small with respect to the size of the structure and is periodic. In most practical applications, however, the microstructure is random. Also, the homogenized stress state $\boldsymbol{\sigma}_0 = \mathbf{E}^0 \nabla \mathbf{u}^0$ can be quite inaccurate and hence cannot be used for damage prediction. It is therefore natural to ask if the homogenized solution can be improved without having to solve the original problem (3). The HDPM provides a systematic way of enhancing the homogenized solution by solving relatively small local problems in areas of high modeling error. These local problems use the exact microstructure information and where necessary, the homogenized solution is used as Dirichlet data.

4.1. Construction of local problems

We first consider a non-overlapping partition \mathcal{P} of the domain Ω into N subdomains Θ_k , $k = 1, 2, \dots, N(\mathcal{P})$ (Fig. 1) such that

$$\bigcup_{k=1}^{N(\mathcal{P})} \bar{\Theta}_k = \bar{\Omega}, \quad \Theta_k \cap \Theta_l = \emptyset, \quad k \neq l. \quad (29)$$

The boundary $\partial \Theta_k$ of each subdomain Θ_k consists of a portion Γ_{k_t} on which tractions are prescribed and a portion Γ_{k_u} on which displacements are prescribed

$$\Gamma_{k_t} = \Gamma_t \cap \partial \Theta_k, \quad \Gamma_{k_u} = \partial \Theta_k \setminus \Gamma_{k_t} \quad (30)$$

Local function spaces are defined as

$$\mathbf{V}(\Theta_k) \stackrel{\text{def}}{=} \{\mathbf{v} : \mathbf{v} \in \mathbf{V}(\Omega), \mathbf{v}|_{\partial \Theta_k} = \mathbf{0}, \mathbf{v}|_{\Gamma_{k_u}} = \mathbf{0}\}. \quad (31)$$

For each subdomain, we define an operator \mathcal{E}_k that extends functions from the local space $\mathbf{V}(\Theta_k)$ to $\mathbf{V}(\Omega)$ as follows:

$$\mathcal{E}_k : \mathbf{V}(\Theta_k) \ni \mathbf{v}_k \rightarrow \mathbf{v} \in \mathbf{V}(\Omega), \mathbf{v}|_{\Theta_k} \stackrel{\text{def}}{=} \mathbf{v}_k, \mathbf{v}|_{\Omega \setminus \Theta_k} = \mathbf{0}. \quad (32)$$

The restriction of the homogenized solution to each subdomain is defined as $\mathbf{u}_k^0 \stackrel{\text{def}}{=} \mathbf{u}^0|_{\Theta_k}$. We denote by $\tilde{\mathbf{u}}_k^0$ the solution to the following boundary value problem

Find $\tilde{\mathbf{u}}_k^0 \in \{\mathbf{u}_k^0\} + \mathbf{V}(\Theta_k)$ such that

$$\mathcal{B}_k(\tilde{\mathbf{u}}_k^0, \mathbf{v}_k) = \mathcal{F}_k(\mathbf{v}_k) \quad \forall \mathbf{v}_k \in \mathbf{V}(\Theta_k),$$

(33)

for $1 \leq k \leq N(\mathcal{P})$ with

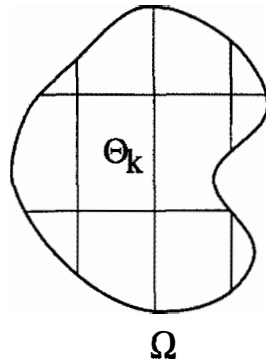


Fig. 1. A non-overlapping partition of the domain.

$$\mathcal{B}_k(\tilde{\mathbf{u}}_k^0, \mathbf{v}_k) \stackrel{\text{def}}{=} \int_{\Theta_k} \nabla \mathbf{v}_k : \mathbf{E} \nabla \tilde{\mathbf{u}}_k^0 \, dx \quad (34)$$

and

$$\mathcal{F}_k(\mathbf{v}_k) \stackrel{\text{def}}{=} \int_{\Theta_k} \mathbf{f} \cdot \mathbf{v}_k \, dx + \int_{\Gamma_{k_i}} \mathbf{t} \cdot \mathbf{v}_k \, ds. \quad (35)$$

The displacements on Γ_{k_u} are prescribed as $\tilde{\mathbf{u}}_k^0|_{\Gamma_{k_u}} = \mathbf{u}_k^0|_{\Gamma_{k_u}}$, i.e. the homogenized solution is used as Dirichlet data on the Γ_{k_u} portion of each subdomain's boundary. In particular, this data is used on the interior part of each subdomain's boundary given by $\partial\Theta \setminus \partial\Omega$. As a result, the local problems are uncoupled. Finally, a global solution is constructed from the local solutions in the following manner

$$\tilde{\mathbf{u}}^0 \stackrel{\text{def}}{=} \mathbf{u}^0 + \sum_{k=1}^{N(\mathcal{P})} \mathcal{E}_k(\tilde{\mathbf{u}}_k^0 - \mathbf{u}_k^0), \quad \tilde{\mathbf{u}}^0 \in \{\hat{\mathbf{u}}\} + \mathbf{V}(\Omega), \quad (36)$$

which will be referred to as the HDPM solution. Clearly, this new solution is continuous across subdomains.

4.2. Characterization of the HDPM solution

We begin by defining the potential energy of functions $\mathbf{w} \in \{\hat{\mathbf{u}}\} + \mathbf{V}(\Omega)$ as

$$\mathcal{J}(\mathbf{w}) \stackrel{\text{def}}{=} \frac{1}{2} \mathcal{B}(\mathbf{w}, \mathbf{w}) - \mathcal{F}(\mathbf{w}). \quad (37)$$

If \mathbf{u} is the exact solution to (3), then it is well known that

$$\mathcal{J}(\mathbf{u}) \leq \mathcal{J}(\mathbf{w}) \quad \forall \mathbf{w} \in \{\hat{\mathbf{u}}\} + \mathbf{V}(\Omega). \quad (38)$$

The following result guarantees that the HDPM solution is indeed an improved solution.

THEOREM 4.1. *With the previous definitions in force,*

$$\mathcal{J}(\tilde{\mathbf{u}}^0) \leq \mathcal{J}(\mathbf{u}^0), \quad (39)$$

and hence

$$\|\mathbf{u} - \tilde{\mathbf{u}}^0\|_{E(\Omega)} \leq \|\mathbf{u} - \mathbf{u}^0\|_{E(\Omega)}. \quad (40)$$

PROOF. See [9]. \square

This result implies that the HDPM solution is always closer to the exact solution than the homogenized solution regardless of the homogenized material properties. Proof of two corollaries that follow immediately from this theorem are in [9]:

COROLLARY 4.1. *Let \mathbf{u} be the exact solution to (3). Additionally, assume that $\nabla \cdot (\mathbf{E} \nabla \tilde{\mathbf{u}}_k^0)$, $\mathbf{f} \in H^{-1}(\Theta_k)$ and $(\mathbf{E} \nabla \tilde{\mathbf{u}}_k^0) \cdot \mathbf{n} \in H^{-1/2}(\Gamma_{k_u})$. Then,*

$$\|\mathbf{u} - \tilde{\mathbf{u}}^0\|_{E(\Omega)}^2 \leq \psi^2 \stackrel{\text{def}}{=} 2(\mathcal{J}(\tilde{\mathbf{u}}^0) - \mathcal{J}(\mathbf{u}^0)) + \zeta^2. \quad (41)$$

This result provides an estimate of the error in the correction $\tilde{\mathbf{u}}^0$ of the homogenized solution. It can be seen that the term $(\mathcal{J}(\tilde{\mathbf{u}}^0) - \mathcal{J}(\mathbf{u}^0))$ is negative so that $\psi \leq \zeta$ always. The next result is a very useful sensitivity property:

COROLLARY 4.2. *Define ζ_k by*

$$\zeta_k^2 \stackrel{\text{def}}{=} \int_{\Theta_k} \mathcal{J}_0 \nabla \mathbf{u}^0 : \mathbf{E} \mathcal{J}_0 \nabla \mathbf{u}^0 \, dx \quad (42)$$

and $\tilde{\mathbf{e}}_k^0$ by $\tilde{\mathbf{e}}_k^0 \stackrel{\text{def}}{=} \tilde{\mathbf{u}}_k^0 - \mathbf{u}_k^0$. Then, for $1 \leq k \leq N(\mathcal{P})$

$$\|\tilde{\mathbf{e}}_k^0\|_{E(\Theta_k)} = \|\tilde{\mathbf{u}}_k^0 - \mathbf{u}_k^0\|_{E(\Theta_k)} \leq \zeta_k \quad (43)$$

The above corollary predicts the improvement that can be obtained by solving a local problem. If ζ_k is small in a subdomain, then there is little gained by solving a local problem. On the other hand, if the above estimate is sharp, and ζ_k is high in a subdomain, the homogenized solution can be significantly improved by solving the local problem (33). We discuss this issue in more detail in the section on numerical examples.

Finally, we present an L^2 estimate of the difference between the HDPM solution and the homogenized solution.

THEOREM 4.2. *Let α_l be as defined in (2). Then, for $1 \leq k \leq N(\mathcal{P})$*

$$\|\tilde{\mathbf{e}}_k^0\|_{L^2(\Theta_k)} = \|\tilde{\mathbf{u}}_k^0 - \mathbf{u}_k^0\|_{L^2(\Theta_k)} \leq \frac{C(\Theta_k)}{\alpha_l} \|\mathbf{E} \mathcal{J}_0 \nabla \mathbf{u}_k^0\|_{L^2(\Theta_k)}, \quad (44)$$

where $C(\Theta_k)$ is constant that only depends on the subdomain Θ_k .

PROOF. The proof is essentially the same as the proof of Theorem 2. First, we note that $\tilde{\mathbf{e}}_k^0$ is the solution to the following boundary value problem on subdomain Θ_k :

Find $\tilde{\mathbf{e}}_k^0 \in V(\Theta_k)$ such that

$$\mathcal{B}_k(\tilde{\mathbf{e}}_k^0, \mathbf{v}_k) = \mathcal{F}_k^0(\mathbf{v}_k) \quad \forall \mathbf{v}_k \in V(\Omega_k)$$

(45)

with the right-hand side

$$\mathcal{F}_k^0(\mathbf{v}_k) = - \int_{\Theta_k} \nabla \mathbf{v}_k : \mathbf{E} \mathcal{J}_0 \nabla \mathbf{u}_k^0 \, d\mathbf{x}. \quad (46)$$

The rest of the steps carry over directly. \square

4.3. The overall algorithm

The overall adaptive algorithm is as follows:

Step 1. Given the initial data $\Omega, \Gamma_u, \Gamma_t, \mathbf{E}, \mathbf{f}, \hat{\mathbf{u}}$ and t , construct a partition of the domain $\mathcal{P} = \{\Theta_k\}_{k=1}^N$. Choose a homogenized material tensor \mathbf{E}^0 . Specify sensitivity and error tolerances α_1 and α_2 so that

$$(\zeta_k)_{\text{tol}} \stackrel{\text{def}}{=} \alpha_1 \|\mathbf{u}^0\|_{E(\Omega)} \times \frac{|\Theta_k|}{|\Omega|}, \quad \psi_{\text{tol}} \stackrel{\text{def}}{=} \alpha_2 \|\mathbf{u}^0\|_{E(\Omega)}. \quad (47)$$

Step 2. Solve the homogenized problem (9) to obtain \mathbf{u}^0 .

Step 3. Compute the local sensitivities ζ_k using (42) for $k = 1, \dots, N(\mathcal{P})$ and form a set \mathcal{J} of subdomains which are above the prescribed sensitivity tolerance

$$\mathcal{J} = \{k : \zeta_k \geq (\zeta_k)_{\text{tol}}\}. \quad (48)$$

Step 4. For the subdomains that fail to satisfy the sensitivity tolerance, $k \in \mathcal{J}$, solve the local problems (33) to obtain $\tilde{\mathbf{u}}_k^0$.

Step 5. Construct the HDPM solution

$$\tilde{\mathbf{u}}^0 = \mathbf{u}^0 + \sum_{k \in \mathcal{J}} \mathcal{E}_k(\tilde{\mathbf{u}}_k^0 - \mathbf{u}_k^0). \quad (49)$$

Step 6. Compute the estimated error in the HDPM solution

$$\psi \stackrel{\text{def}}{=} [2(\mathcal{J}(\tilde{\mathbf{u}}^0) - \mathcal{J}(\mathbf{u}^0)) + \zeta^2]^{1/2} \quad (50)$$

Step 7. If $\psi \leq \psi_{\text{tol}}$, STOP. Else, repeat Steps 2–7 with improved material properties. A general algorithm for

choosing improved properties can be found in [9]. If the error tolerance is not satisfied with improved material properties, go to Step 8.

Step 8. Coarsen the partition and repeat Steps 2–7.

Step 9. Relaxation. (This step is optional). At the conclusion of the adaptive process when all global and subdomain errors meet the assigned tolerances, tractions are discontinuous across subdomain boundaries. A number of Schwarz-type iterations relaxing the boundary constraints on displacements can be performed to reduce the stress discontinuity, remove spurious singularities in the displacement derivatives, and further improve the accuracy of local features of the solution.

REMARK 4.1. While in principle, it is possible to use traction boundary conditions to solve the local problems, the need for flux-equilibration introduces certain difficulties. Moreover, the final solution may not be continuous across subdomains. The use of Dirichlet boundary conditions obviates these complications and allows for easy parallel solution of the local problems [11].

REMARK 4.2. There is a considerable amount of literature on the use of global–local and multiscale analyses for modeling heterogeneous materials. This includes the works of Fish and Belsky [3,4], Ghosh and Moorthy [5], Ghosh and Mukhopadhyay [6] and more recently Moës et al. [7]. In the HDPM, the effects of multiple scales are automatically included in the analysis by allowing the a posteriori estimates to choose the most appropriate scales. The coarsening of the partition in Step 8 of the overall adaptive algorithm above corresponds to an increase in the disparity between scales.

5. Homogenization error in quantities of interest

Recent work in error estimation in the context of finite element analysis has focused on obtaining bounds on the numerical error in quantities of interest other than the energy norm [1,10]. In this section, we use the approach of Prudhomme and Oden [10] to obtain an upper bound on the homogenization error in other quantities. We assume that we are interested in estimating $L(\mathbf{e}^\bullet) = L(\mathbf{u}) - L(\mathbf{u}^\bullet)$, where L is a continuous linear functional on $V(\Omega)$, $L \in V'$. For instance, L may represent something more localized than the global estimate (12) such as the error in \mathbf{u} or $\nabla \mathbf{u}$ over a small region in Ω . The main objective here is to relate $L(\mathbf{e}^\bullet)$ to the ‘source’ of the homogenization error, the right-hand side of (16). So, we would like to find a linear functional $\mathcal{W} \in V''$, if it exists, such that

$$L(\mathbf{e}^\bullet) = \mathcal{W}(\mathcal{R}^\bullet) = \langle \mathcal{W}, \mathcal{R} \rangle_{V'' \times V'} . \quad (51)$$

The functional \mathcal{W} is known as the influence function(al) since it indicates the influence of the residual on the quantity of interest. Since, V is reflexive, we have that $\exists ! \boldsymbol{\omega} \in V$ such that

$$\langle \mathcal{R}, \boldsymbol{\omega} \rangle_{V' \times V} = \langle \mathcal{W}, \mathcal{R} \rangle_{V'' \times V'} . \quad (52)$$

and hence (51) becomes

$$L(\mathbf{e}^\bullet) = \mathcal{R}^\bullet(\boldsymbol{\omega}) . \quad (53)$$

Using (16), we obtain

$$L(\mathbf{e}^\bullet) = \mathcal{B}(\mathbf{e}^\bullet, \boldsymbol{\omega}) . \quad (54)$$

The influence function $\boldsymbol{\omega}$ can thus be obtained as a solution to the global dual problem

<p>Find $\boldsymbol{\omega} \in V(\Omega)$ such that</p> $\mathcal{B}(\mathbf{v}, \boldsymbol{\omega}) = L(\mathbf{v}) \quad \forall \mathbf{v} \in V(\Omega) .$	(55)
--	------

It then follows that $\boldsymbol{\omega}$ exists and is unique. The dual problem (55), however, is as difficult to solve as the original problem (3). A natural way to simplify this problem is to solve the homogenized dual problem

$$\boxed{\begin{aligned} &\text{Find } \boldsymbol{\omega}^\bullet \in V(\Omega) \text{ such that} \\ &\mathcal{B}^0(\mathbf{v}, \boldsymbol{\omega}^0) = L(\mathbf{v}) \quad \forall \mathbf{v} \in V(\Omega). \end{aligned}} \quad (56)$$

It immediately follows that the modeling error in the influence function $\bar{\mathbf{e}}^0 \stackrel{\text{def}}{=} \boldsymbol{\omega} - \boldsymbol{\omega}^0$ satisfies

$$\boxed{\mathcal{B}(\mathbf{v}, \bar{\mathbf{e}}^0) = \bar{\mathcal{R}}^0(\mathbf{v}) \quad \forall \mathbf{v} \in V(\Omega),} \quad (57)$$

with

$$\bar{\mathcal{R}}^0(\mathbf{v}) = - \int_{\Omega} \nabla \boldsymbol{\omega}^0 : \mathbf{E} \mathcal{J}_\bullet \nabla \mathbf{v} \, dx. \quad (58)$$

We also note that $\bar{\mathbf{e}}^0$ satisfies the following bound (analogous to (12)):

$$\|\bar{\mathbf{e}}^0\|_{E(\Omega)}^2 = \|\boldsymbol{\omega} - \boldsymbol{\omega}^0\|_{E(\Omega)}^2 \leq \bar{\zeta}^2 \stackrel{\text{def}}{=} \int_{\Omega} \mathcal{J}_0 \nabla \boldsymbol{\omega}^0 : \mathbf{E} \mathcal{J}_\bullet \nabla \boldsymbol{\omega}^0 \, dx. \quad (59)$$

Next, we note that

$$L(\mathbf{e}^0) = \mathcal{B}(\mathbf{e}^\bullet, \boldsymbol{\omega}) = \mathcal{B}(\mathbf{e}^0, \bar{\mathbf{e}}) + \mathcal{B}(\mathbf{e}^0, \boldsymbol{\omega}^0) \quad (60)$$

and hence

$$\begin{aligned} |L(\mathbf{e}^0)| &\leq |\mathcal{B}(\mathbf{e}^\bullet, \bar{\mathbf{e}})| + |\mathcal{B}(\mathbf{e}^0, \boldsymbol{\omega}^0)| \\ &\leq \|\mathbf{e}^0\|_{E(\Omega)} \|\bar{\mathbf{e}}^0\|_{E(\Omega)} + \|\mathbf{e}^0\|_{E(\Omega)} \|\boldsymbol{\omega}^0\|_{E(\Omega)}. \end{aligned} \quad (61)$$

Finally, using (12) and (59), we arrive at the following bound for the homogenization error in the quantity of interest,

$$\boxed{|L(\mathbf{e}^0)| \leq \beta \stackrel{\text{def}}{=} \zeta \bar{\zeta} + \zeta \|\boldsymbol{\omega}^0\|_{E(\Omega)}} \quad (62)$$

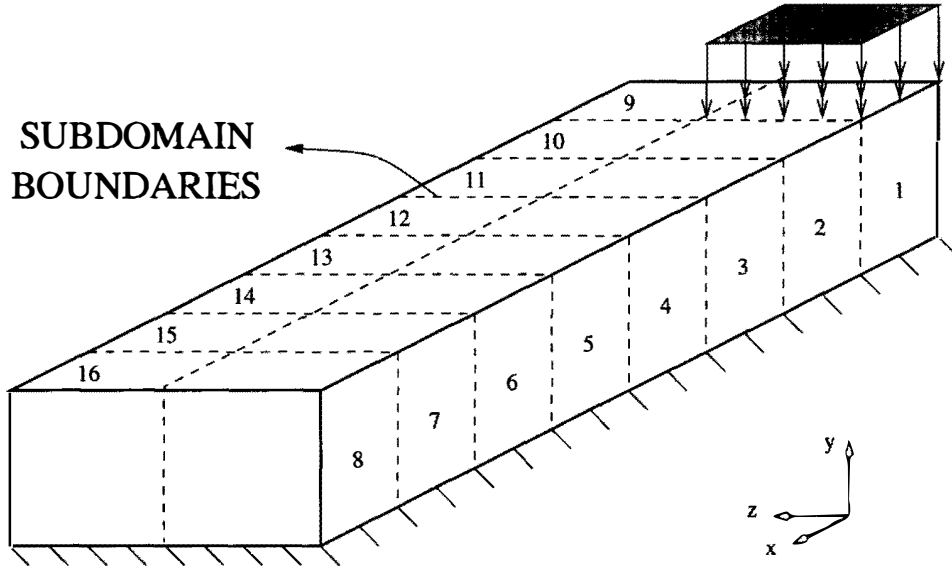
Thus, the estimation of the homogenization error in the quantity of interest requires the solution of a global dual problem. In our analysis above, we assume that the homogenization parameters chosen for the dual problem are the same as the ones chosen for the primal (original) problem. As a result, the two problems have the same left-hand side which is computationally convenient. This assumption, however, can be relaxed without major changes to our analysis. Indeed, this may not be an unattractive choice considering the fact that the homogenized problem typically requires far fewer degrees of freedom than a local problem with microstructure (see Example 6.1). Later in this paper, we present some 1-D examples to illustrate the performance of our estimate.

6. Numerical examples

6.1. Example 1

Consider a composite slab (dimensions $8 \times 1 \times 2$) divided into 16 equal subdomains. The body is subjected to a uniform compressive load over one subdomain as shown in Fig. 2. We assume that the microstructure is provided by 1024 spherical inclusions distributed uniformly in the matrix material so that each subdomain has a $4 \times 4 \times 4$ arrangement of inclusions (Fig. 3). While the matrix has the properties $E = 400.0$ MPa, $\nu = 0.2$, the inclusions have the properties $E = 4000.0$ MPa, $\nu = 0.2$. The volume fraction of the inclusions is assumed to be 0.2. To obtain the homogenized material properties, we use the arithmetic average of the Hashin–Shtrikman bounds. Finally, we use $(\zeta_k)_{\text{tot}} = 0.5 \|\mathbf{u}^\bullet\|_{E(\Omega)} \times |\mathcal{Q}_k|/|\Omega|$.

An approximation to \mathbf{u}^0 is generated using the adaptive hp finite element program ProPHLEX [2] and is denoted by $\mathbf{u}^{\bullet,H}$. The hp mesh used to solve the homogenized problem (see Fig. 4) has 7407 degrees of freedom with an estimated relative numerical error of 4.0% in the energy norm.



DIMENSIONS : 8x1x2

Fig. 2. Schematic of the composite bar partitioned into 16 subdomains. Subdomain numbering is also shown.

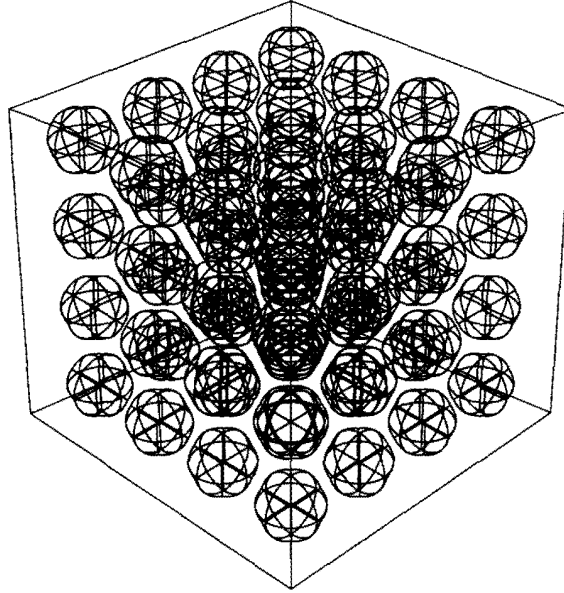
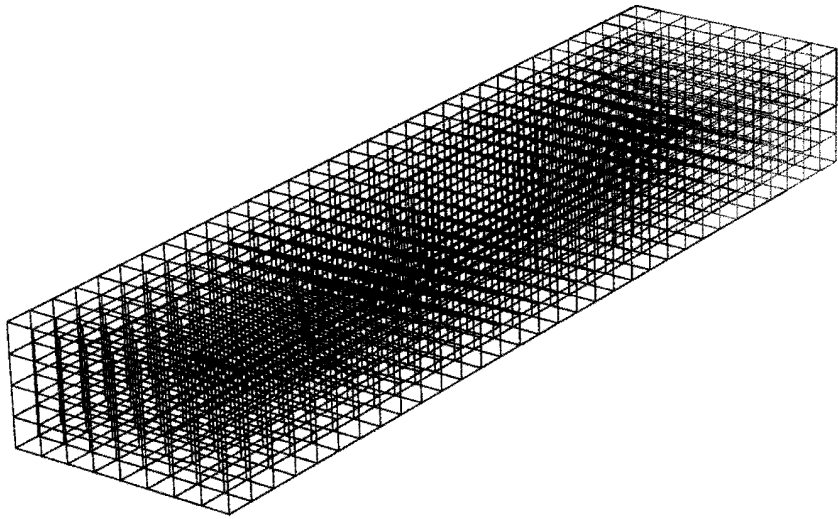


Fig. 3. The microstructure in each subdomain.

On computing the ζ_k , $1 \leq k \leq 16$, it is found that 4 subdomains fail to satisfy the sensitivity criterion (see (48)) so that $\mathcal{J} = \{1, 2, 9, 10\}$. In these subdomains, we find approximate solutions to the local problems (33), $k \in \mathcal{J}$ and denote these by $\tilde{\mathbf{u}}_k^{0,h}$. The hp mesh for subdomain 1 is shown in Fig. 5. The HDPM solution is constructed using

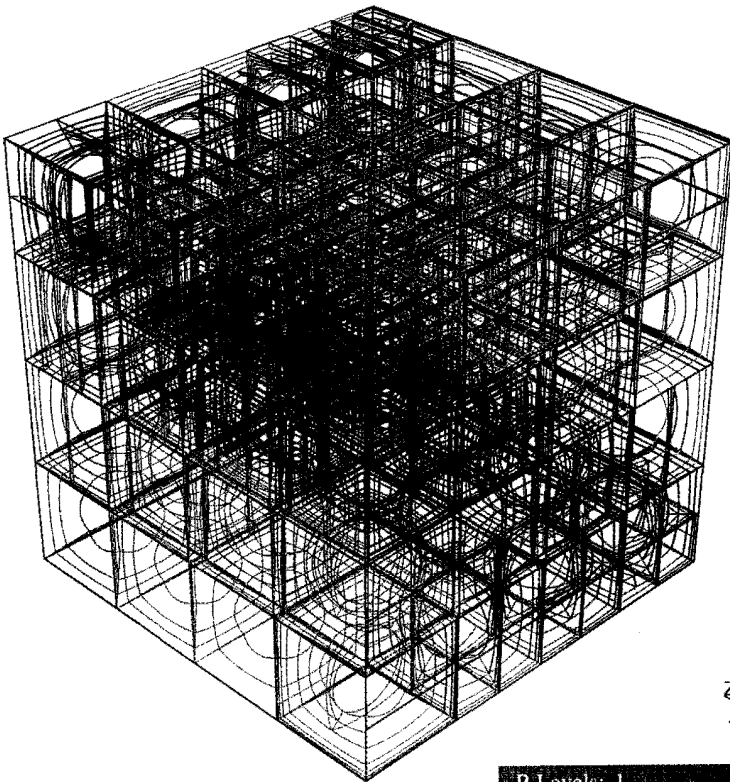
$$\tilde{\mathbf{u}}^{0,h,H} = \mathbf{u}^{0,H} + \sum_{k \in \mathcal{J}} \mathcal{E}_k(\tilde{\mathbf{u}}_k^{0,h} - \mathbf{u}_k^{0,H}). \quad (63)$$

It is found that $\zeta^H / \|\mathbf{u}^0\|_{E(\Omega)} = 0.604$ and $\psi^{h,H} / \|\mathbf{u}^0\|_{E(\Omega)} = 0.065$. Thus, the HDPM can dramatically improve the homogenized solution.



P-Levels: 1 8

Fig. 4. *hp* mesh for the homogenized problem with 7407 degrees of freedom.



P-Levels: 1 8

Fig. 5. *hp* mesh for subdomain 1 with 93 261 degrees of freedom.

A quantity that is of interest in stress analysis is the Von-Mises stress. The maximum Von-Mises stress (see Fig. 6) predicted by the homogenized problem is 170.3 MPa at $\mathbf{x} = \mathbf{0}$ whereas the maximum Von-Mises stress predicted by the HDPM solution is 534.98 MPa in subdomain 1 at $\mathbf{x} = (0.177, 0.072, 0.072)$ (see Fig. 7). Thus the use of the homogenized solution for making design decisions without further processing can be quite dangerous.

Finally, we note that the homogenized problem needs 7407 degrees of freedom and each local problem on an average requires about 90 000 degrees of freedom. For this problem, it is estimated that a direct simulation requires about 1 800 000 degrees of freedom.

6.2. Example 2

Now, we consider an example focusing on the difficulties posed by the highly oscillatory nature of \mathbf{E} , the most significant of these being the integration of functions of \mathbf{E} . One such quantity is the local sensitivity indicator (42).

We choose the problem of a beam clamped to a wall at one end and loaded by tractions on the other end. The beam has reinforcing bars as shown in Fig. 8. The mismatch ratio of the two materials is assumed to be 5.0. We homogenize the beam using the Hashin–Shtrikman bounds and then compute an approximation to the homogenized solution \mathbf{u}^0 . The next step is to compute

$$\zeta_k \stackrel{\text{def}}{=} \left\{ \int_{\bullet_k} \mathcal{J}_{\bullet} \nabla \mathbf{u}^0 : \mathbf{E} \mathcal{J}_{\bullet} \nabla \mathbf{u}^0 \, d\mathbf{x} \right\}^{1/2}, \quad (64)$$

and

$$\zeta = [\sum \zeta_k^2]^{1/2}. \quad (65)$$

Obviously, the integrands above are highly oscillatory. We use two methods to evaluate the above expressions.

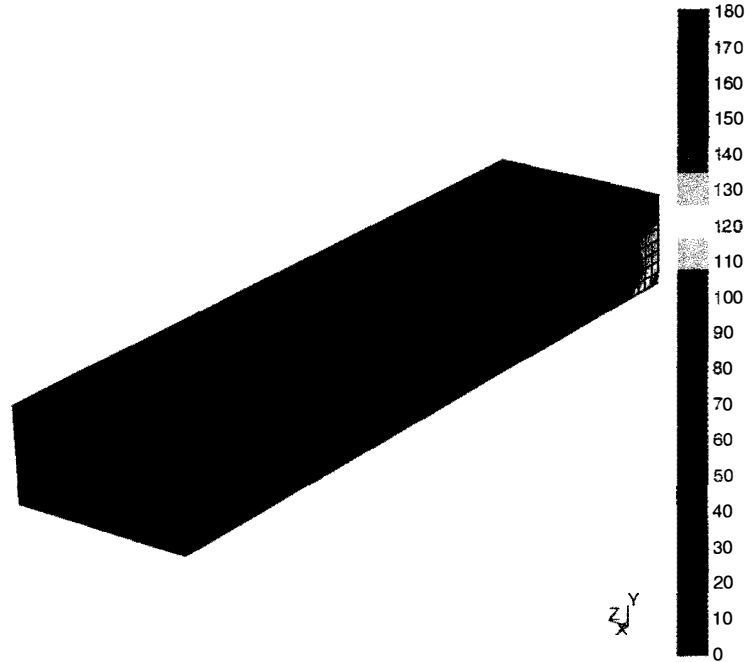


Fig. 6. Von-Mises stress field on the exterior of composite body. Maximum stress predicted by the homogenized problem is 170.3 MPa.

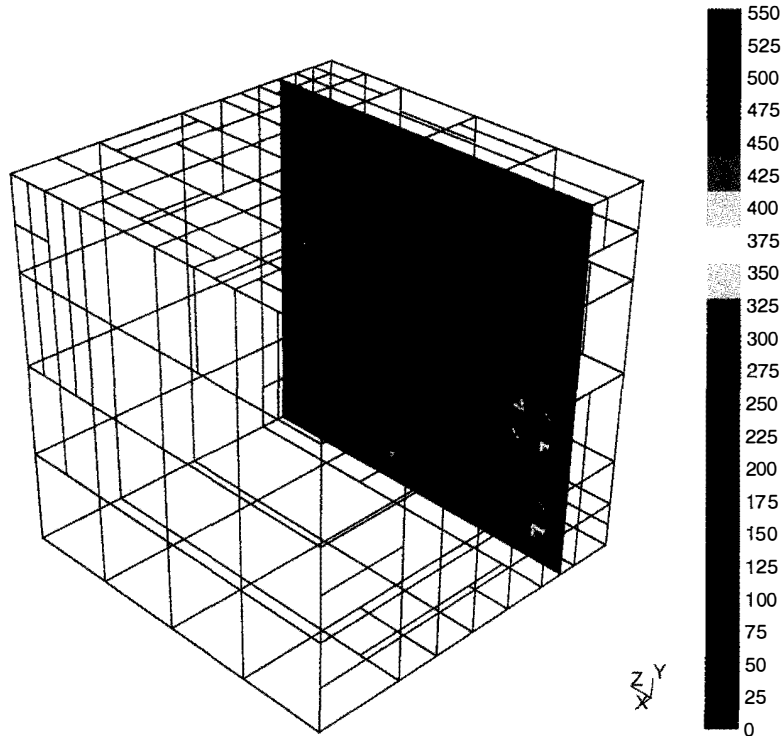


Fig. 7. Von-Mises stress field on a slice of subdomain 1. Maximum stress predicted by local analysis is 534.98 MPa.

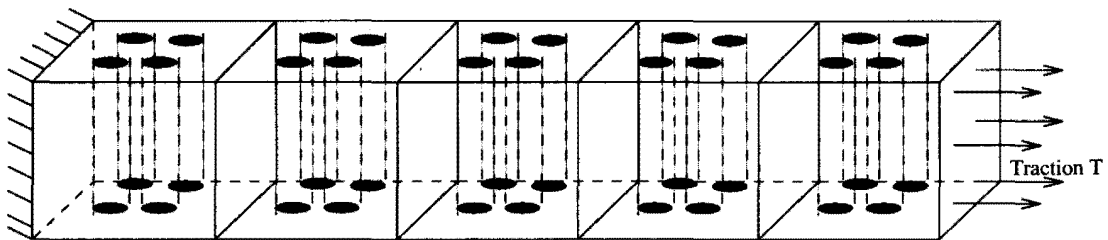
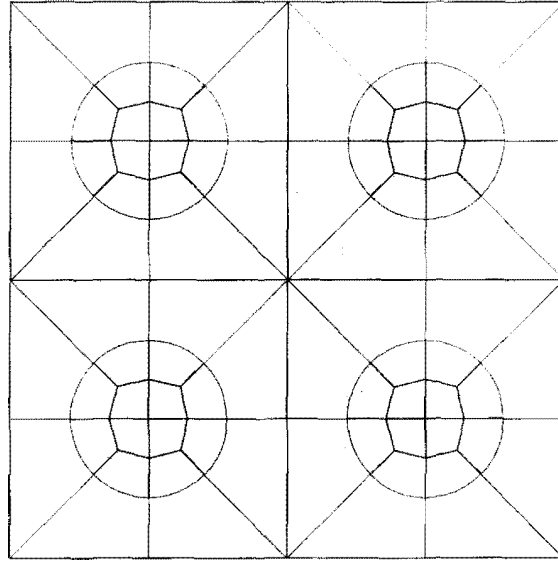


Fig. 8. Schematic of a reinforced beam clamped at one end and loaded on the other end.

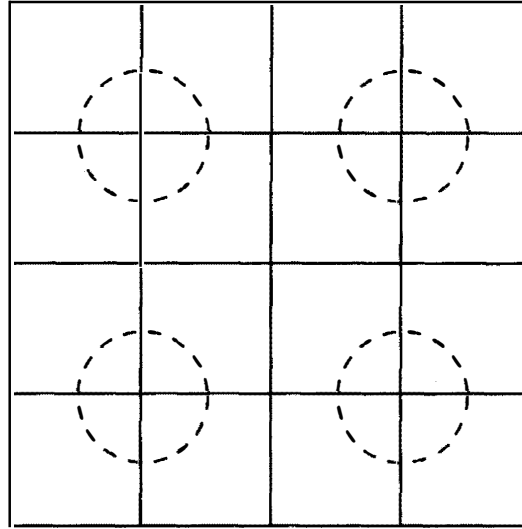
In the first method, we use a conforming mesh that respects the boundaries of the microstructure as shown in Fig. 9(a) and in the second method, we use a uniform mesh as in Fig. 9(b). The two methods are compared for Gaussian integration rules varying from the $1 \times 1 \times 1$ integration rule to the $10 \times 10 \times 10$ integration rule in each element. In the first case, the material properties are known element-wise and in the second, it is necessary to check if a given integration point lies in the matrix or an inclusion. From Fig. 10, we see that the result obtained using a non-conforming mesh is highly oscillatory both for $\zeta_{k=1}$ and ζ . This shows that the use of conforming meshes, though expensive due to time spent in mesh generation, is necessary for integrating highly oscillatory functions. On the other hand, non-conforming meshes are relatively easier to generate but the number of integration points per element required for accurate results make their use an unattractive choice.

6.3. Example 3

We now present a preliminary study on the performance of the estimate (62) for the following 1-D problem. Consider an elastic bar of unit length fixed at both ends and subjected to a constant body force. The primal fine-scale and homogenized problems are



(a)



(b)

Fig. 9. (a) Conforming and (b) non-conforming meshes for computing ζ_k and ζ .

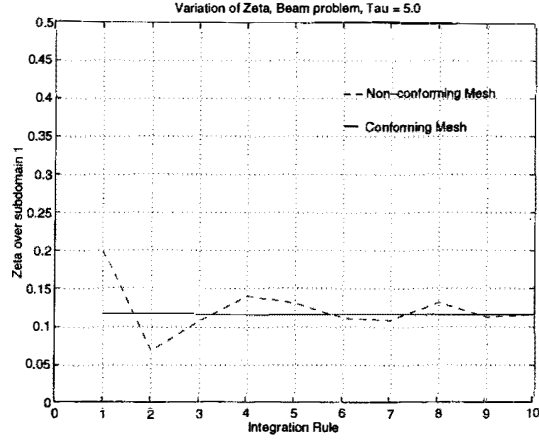
$$-\frac{d}{dx} \left(E(x) \frac{du}{dx} \right) = -1, \quad u(0) = 0, \quad u(1) = 0 \quad (66)$$

and

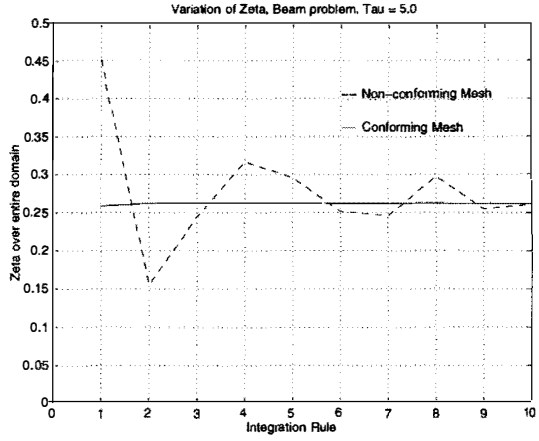
$$-\frac{d}{dx} \left(E_p^0(x) \frac{du^0}{dx} \right) = -1, \quad u^0(0) = 0, \quad u^0(1) = 0. \quad (67)$$

Here, E_p^0 indicates the homogenization parameter for the primal problem. The first linear functional we consider (as indicated by the subscript 1) is

$$L_1(v) = v(x_0), \quad x_0 \in (0, 1) \quad (68)$$



(a)



(b)

Fig. 10. Variation of (a) $\zeta_{k=1}$ and (b) ζ with integration rule.

meaning that we are interested in pointwise values of the homogenization error. The dual fine-scale and homogenized problems therefore are

$$-\frac{d}{dx} \left(E(x) \frac{dw_1}{dx} \right) = \delta(x - x_0), \quad w_1(0) = 0, \quad w_1(1) = 0 \quad (69)$$

and

$$-\frac{d}{dx} \left(E_d^0(x) \frac{dw_1^0}{dx} \right) = \delta(x - x_0), \quad w_1^0(0) = 0, \quad w_1^0(1) = 0, \quad (70)$$

with the subscript d indicating the dual problem. In this case, the influence function w_1 is the Green's function of the operator $-d/dx(E(x)d/dx(\cdot))$. Thus, our approach can be viewed as a generalization of the Green's function approach. The second linear functional we consider is given by

$$L_2(v) = \int_a^b v(x) dx, \quad (a, b) \subset (0, 1). \quad (71)$$

Here, we are interested in the average values of the homogenization error over regions of the unit interval. The dual fine-scale and homogenized problems in this case are

$$-\frac{d}{dx} \left(E(x) \frac{dw_2}{dx} \right) = H(x - a) - H(x - b), \quad w_2(0) = 0, \quad w_2(1) = 0 \quad (72)$$

and

$$-\frac{d}{dx} \left(E_d^0(x) \frac{dw_2^0}{dx} \right) = H(x-a) - H(x-b), \quad w_2^0(0) = 0, \quad w_2^0(1) = 0. \quad (73)$$

The unit interval is divided into 1000 equal intervals, and for each interval the material property is chosen at random to be either $E = 1$ or $E = \tau$, where τ is the mismatch ratio. Equal amounts of hard and soft material are used. All of the following calculations are performed analytically. Also, E_p^0 and E_d^0 are independently chosen to be the arithmetic average $\langle E \rangle$ or the harmonic average $\langle E^{-1} \rangle^{-1}$. Finally, we define the effectivity index by $\eta \stackrel{\text{def}}{=} |L(e^0)|/\beta$.

From Tables 1 and 2 it is seen that when the harmonic average is chosen to homogenize the primal problem, pointwise errors are very small but the estimate performs poorly. The poor performance results from the fact that the estimate (62) does not account for any cancellations. On the other hand, when the arithmetic average is chosen to homogenize the primal problem, pointwise errors are high and the estimate performs relatively well. The effect of cancellations is not very significant in this case. In either case, using the arithmetic average for the dual problem improves the estimate.

6.4. Example 4

In the final example of this paper, we demonstrate a simple scheme for the study of damage mechanics of composites in the framework of hierarchical modeling. We consider a unit cube of material, with a two-phase isotropic spherical microstructure (see Fig. 11). The volume fraction of the inclusion material is 0.25 and the material properties are chosen to be those used in Example 1. The cube is fixed on the face $y = 0$ and loaded by shear on the face $y = 1$. We employ a unidirectional partitioning of the cube into four simple ‘slabs’: $0 < \Theta_1 < 1/4$, $1/4 < \Theta_2 < 2/4$, $2/4 < \Theta_3 < 3/4$, and $3/4 < \Theta_4 < 1$. The homogenized parameters are

Table 1
Effectivity indices for $L_1(v) = v(x_0)$, $x_0 = 0.67$

τ	E_p^0	E_d^0	$L_1(e)$	β	η
10.0	$\langle E^{-1} \rangle^{-1}$	$\langle E^{-1} \rangle^{-1}$	0.000214	0.3369	1570.5
10.0	$\langle E^{-1} \rangle^{-1}$	$\langle E \rangle$	0.000214	0.1480	689.9
10.0	$\langle E \rangle$	$\langle E^{-1} \rangle^{-1}$	-0.0405	0.1935	4.8
10.0	$\langle E \rangle$	$\langle E \rangle$	-0.0405	0.085	2.1
100.0	$\langle E^{-1} \rangle^{-1}$	$\langle E^{-1} \rangle^{-1}$	0.000236	3.405	14428.5
100.0	$\langle E^{-1} \rangle^{-1}$	$\langle E \rangle$	0.000236	0.399	1691.9
100.0	$\langle E \rangle$	$\langle E^{-1} \rangle^{-1}$	-0.0534	0.6733	12.6
100.0	$\langle E \rangle$	$\langle E \rangle$	-0.0534	0.0789	1.5

Table 2
Effectivity indices for $L_2(v) = \int_a^b v dx$, $a = 0.45$, $b = 0.50$

τ	E_p^0	E_d^0	$L_2(e)$	β	η
10.0	$\langle E^{-1} \rangle^{-1}$	$\langle E^{-1} \rangle^{-1}$	0.0000067	0.0175	2610.0
10.0	$\langle E^{-1} \rangle^{-1}$	$\langle E \rangle$	0.0000067	0.0077	1150.2
10.0	$\langle E \rangle$	$\langle E^{-1} \rangle^{-1}$	-0.00229	0.01	4.4
10.0	$\langle E \rangle$	$\langle E \rangle$	-0.00229	0.0044	1.9
100.0	$\langle E^{-1} \rangle^{-1}$	$\langle E^{-1} \rangle^{-1}$	0.0000074	0.1772	23966.4
100.0	$\langle E^{-1} \rangle^{-1}$	$\langle E \rangle$	0.0000074	0.0209	2825.3
100.0	$\langle E \rangle$	$\langle E^{-1} \rangle^{-1}$	-0.00301	0.0350	11.6
100.0	$\langle E \rangle$	$\langle E \rangle$	-0.00301	0.0041	1.37

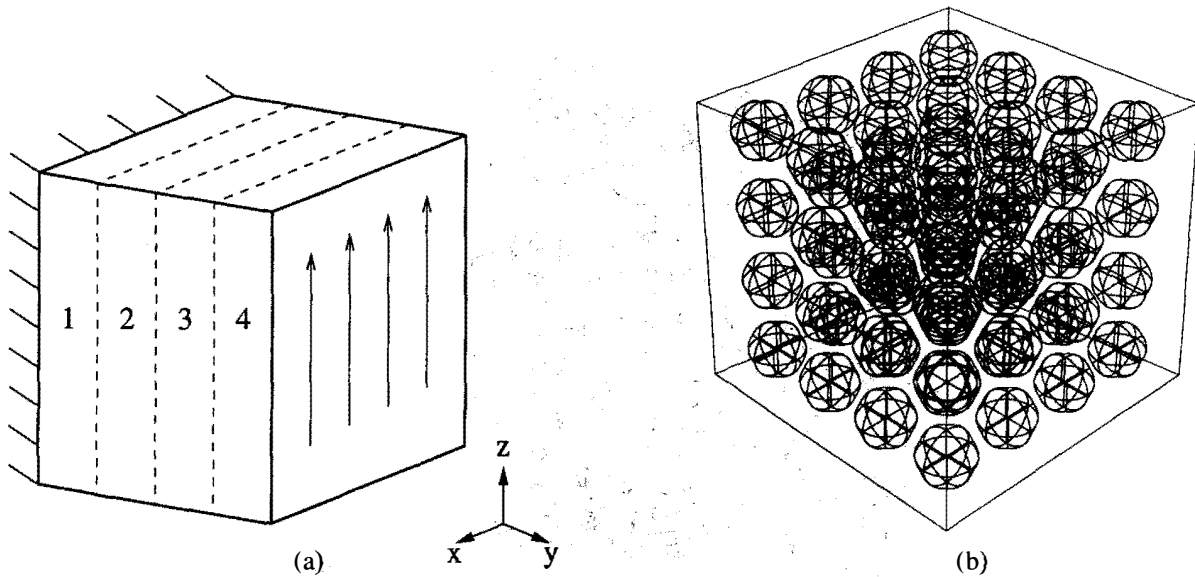


Fig. 11. Schematic of (a) the composite cube and (b) the microstructure employed in studying damage mechanics.

generated using the arithmetic average of the Hashin–Shtrikman bounds and the homogenized problem is solved *hp* adaptively to obtain $\mathbf{u}^{0,H}$.

Now, we wish to study the initiation and propagation of damage in each of the subdomains Θ_k , $1 \leq k \leq 4$. This is done using the following algorithm:

Step 1. Set iteration count to 0.

Step 2. Solve the local problem (33) to obtain $\tilde{\mathbf{u}}_k^{0,h}$ for this iteration.

Step 3. Loop over the elements of the mesh and compute the maximum Von-Mises stress in each element. If this is greater than a preset limit, disable the element by setting the stiffness of the element to a very small number.

Step 4. If the number of elements that fail the test in Step 3 is >0 , increment the iteration count and GOTO Step 2. Else, STOP.

The process of ‘disabling’ elements leads to a redistribution of stresses and the new stress state may or may not satisfy the failure criterion. In case the criterion is not satisfied, the above algorithm can be carried out until a certain volume fraction of the subdomain has failed. Note that Step 3 in the algorithm above can be modified to include other failure modes such as debonding by considering different failure criteria. The essential idea is that these analyses can be performed in the context of hierarchical modeling.

The above algorithm is applied to subdomain 4. We assume that the inclusion material fails at 490.0 MPa and the matrix material fails at 400.0 MPa. Fig. 12 shows two views, A and B, of the Von-Mises stress distribution in the subdomain at the zeroth iteration, i.e. before the initiation of damage. View B is obtained by rotating view A by 180° about the z axis. It is found that the maximum Von-Mises stress at this iteration is 497.24 MPa. Four inclusion elements and 8 matrix elements fail the tolerance test (Step 3 above). These elements are disabled and the problem is resolved. The Von-Mises stress field for iteration 1 is shown in Fig. 13. Now the maximum Von-Mises stress in the subdomain increases to 968.58 MPa and 46 elements fail the tolerance test. After another iteration, we see the propagation of damage in the inclusions more clearly (Fig. 14). The maximum Von-Mises stress in the subdomain is now 1194.79 MPa.

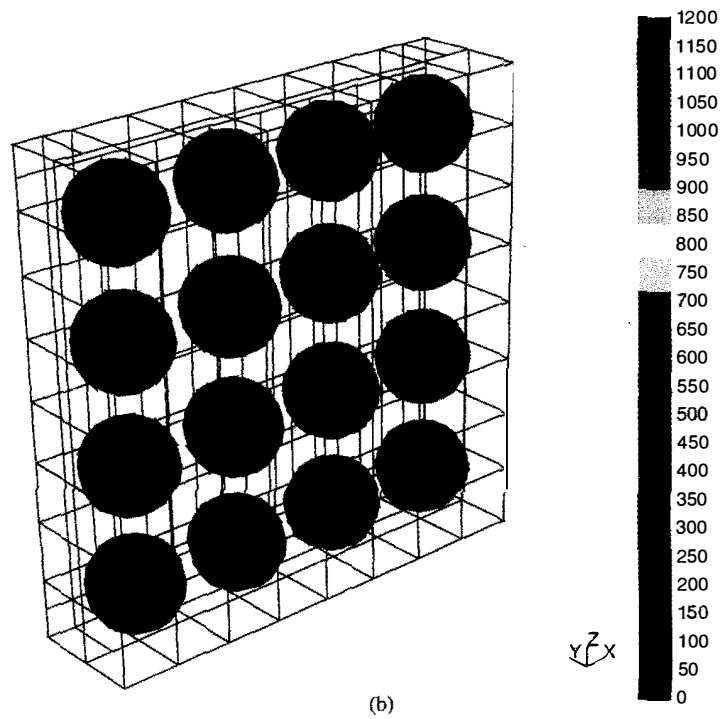
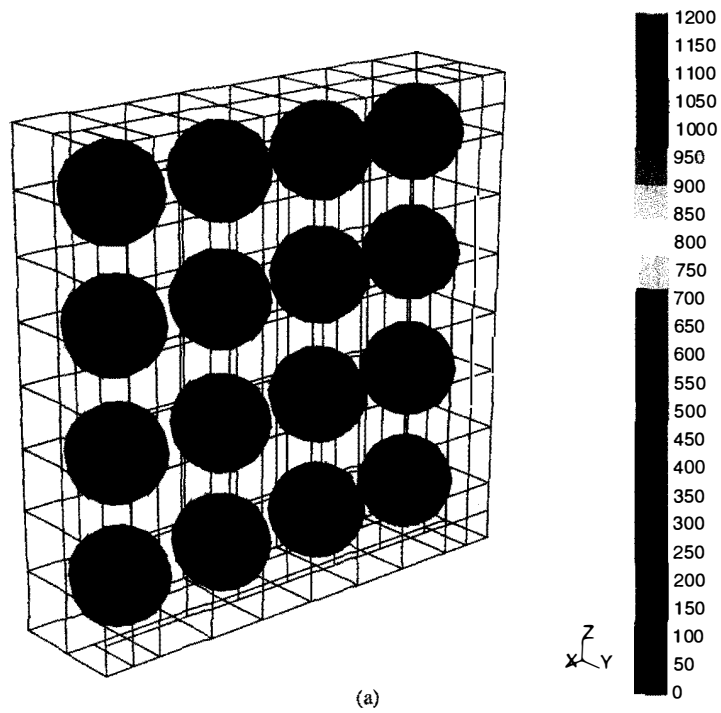


Fig. 12. Von-Mises stress distribution on the inclusions in subdomain 4 at iteration 0, (a) View A and (b) View B.

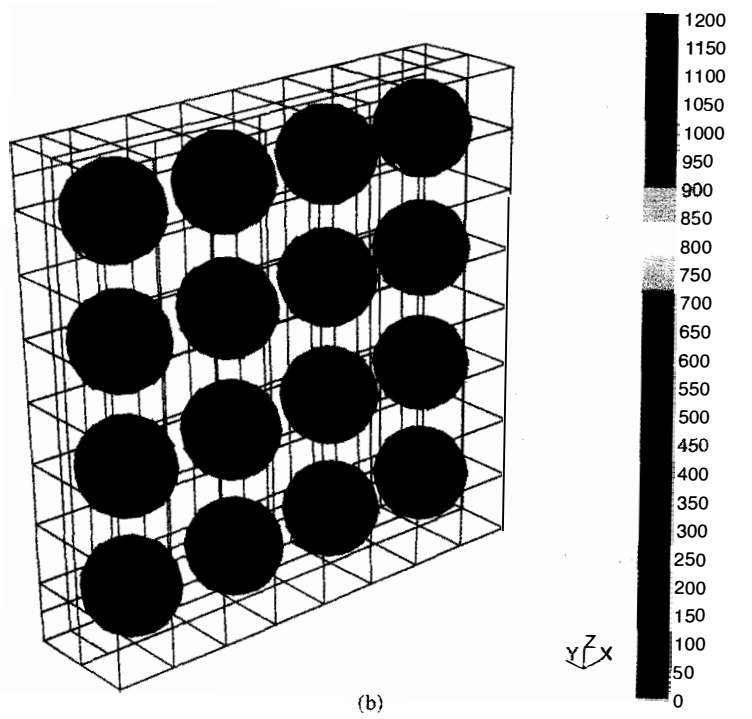
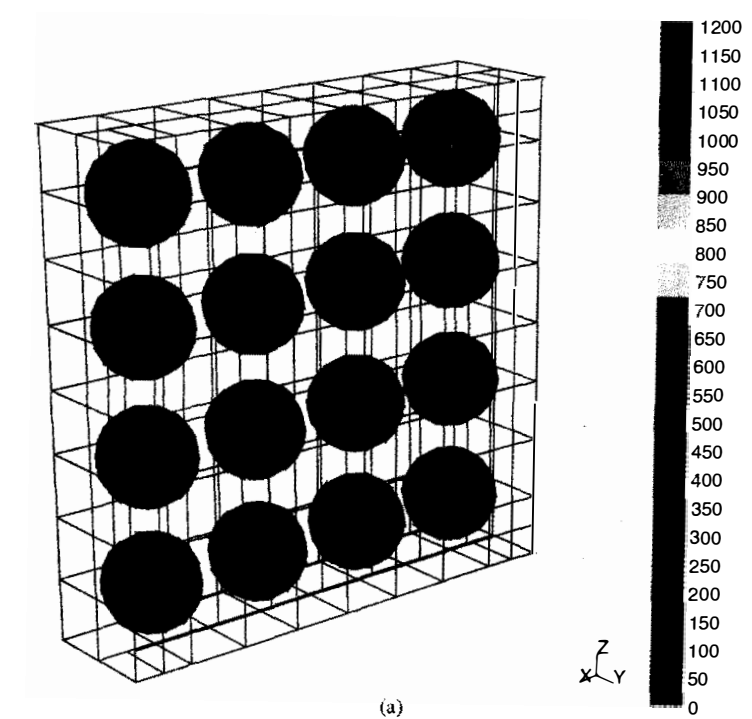


Fig. 13. Von-Mises stress distribution on the inclusions in subdomain 4 at iteration 1, (a) View A and (b) View B.

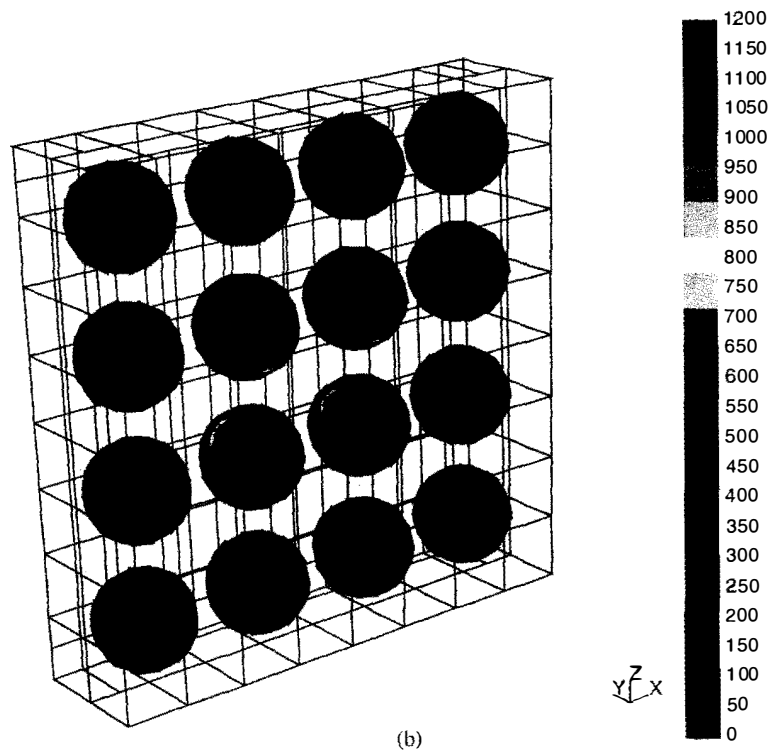
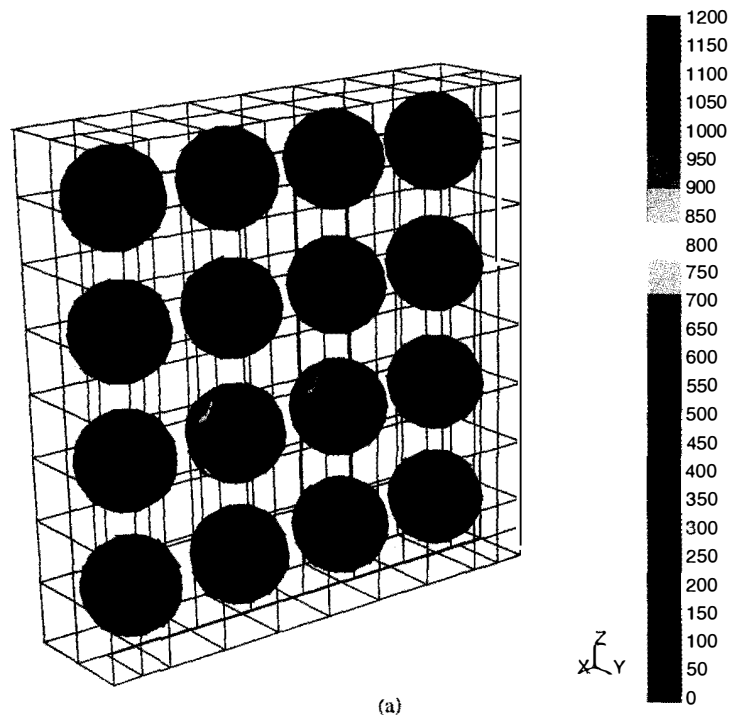


Fig. 14. Von-Mises stress distribution on the inclusions in subdomain 4 at iteration 2, (a) View A and (b) View B.

7. Final comments

The concept of hierarchical modeling, and its implementation through the Homogenized Dirichlet Projection Method, provide a systematic family of approaches toward the resolution of multiscale problems, particularly problems of analyzing heterogeneous materials. The approach bypasses or generalizes many of the traditional limitations of homogenization theory and the theory of composite materials. To mention a few:

- no periodicity of microscale constituents is assumed
- the approach (therefore) does not rely on the existence of RVEs (Representative Volume Elements)
- homogenization methods are merely artifacts of the overall adaptive strategy and are not goals of the modeling process in themselves (however, the choice of homogenization technique has significant impact on the performance of error estimators and the success of the method)
- extensions to multiscale modeling problems are possible
- as shown in the present study, nonlinear behavior can be accommodated in the modeling process in a straightforward manner, albeit at more computational expense.

A number of extensions and generalizations of the hierarchical modeling concept represent challenging but critical areas for future work and some of these are currently under study. These include the development of adaptive modeling strategies more integrated with the homogenization steps to allow for systematic modeling of multiscale phenomena. These could be used to control multiple (internal) iterations of the HDPM strategy to address many different levels of scales present in many applications. More work is needed to refine our approach to local error estimation and to study the limitations of the approach for model error analysis described here. Finally, modeling of a wide range of nonlinear phenomena is within reach, including a more general simulation of progressive damage accumulation, crack initiation and propagation, life cycle prediction and micromechanical effects, such as local diffusion phenomena. We plan to explore these issues more deeply in future works.

Acknowledgments

We gratefully acknowledge the support of this work by the Office of Naval Research under grant N00014-95-1-0401 and by NSF through NPACI, the National Partnership for Advanced Computational Infrastructure, grant 10152711.

References

- [1] I. Babuska, T. Strouboulis, C.S. Upadhyay and S.K. Gangaraj, A posteriori estimation and adaptive control of the pollution error in the h -version of the finite element method, *Int. J. Numer. Methods Engrg.* 38 (1995) 4207–4235.
- [2] Computational Mechanics Company, Inc., Austin, TX, ProPHLEX User Manual for Version 2.0, 1996.
- [3] J. Fish and V. Belsky, Multigrid method for periodic heterogeneous media. Part 1: Convergence studies for one-dimensional case, *Comput. Methods Appl. Mech. Engrg.* 126 (1995) 1–16.
- [4] J. Fish and V. Belsky, Multigrid method for periodic heterogeneous media. Part 2: Multiscale modeling and quality control in multidimensional case, *Comput. Methods Appl. Mech. Engrg.* 126 (1995) 17–38.
- [5] S. Ghosh and S. Moorthy, Elastic-plastic analysis of arbitrary heterogeneous materials with the voronoi cell finite element method, *Comput. Methods Appl. Mech. Engrg.* 121 (1995) 373–409.
- [6] S. Ghosh and S.N. Mukhopadhyay, A material based finite element analysis of heterogeneous media involving Dirichlet tessellations, *Comput. Methods Appl. Mech. Engrg.* 104 (1993) 211–247.
- [7] N. Moës, J.T. Oden and K. Vemaganti, A two-scale strategy and a posteriori error estimation for modeling heterogeneous structures, in: P. Ladevèze and J.T. Oden, eds., *On New Advances in Adaptive Computational Methods in Mechanics* (Elsevier publication, 1997) to appear.
- [8] N. Moës, J.T. Oden and T.I. Zohdi, Investigation of the interactions between the numerical and the modeling errors in the homogenized Dirichlet projection method, *Comput. Methods Appl. Mech. Engrg.*, to appear.
- [9] J.T. Oden and T.I. Zohdi, Analysis and adaptive modeling of highly heterogeneous elastic structures, *Comput. Methods Appl. Mech. Engrg.* 148 (1997) 367–391.
- [10] S. Prudhomme and J.T. Oden, Goal oriented adaptivity and local error estimation and control, TICAM Report, to appear.
- [11] P. Le Tallec, *Domain decomposition methods in Computational Mechanics* (North-Holland, 1994).
- [12] T.I. Zohdi, *Error estimation and adaptive methods for the analysis of elastic structures composed of highly heterogeneous media*, Ph.D. Thesis, The University of Texas at Austin, 1997.
- [13] T.I. Zohdi, J.T. Oden and G.J. Rodin, Hierarchical modeling of heterogeneous bodies, *Comput. Methods Appl. Mech. Engrg.* 138 (1996) 273–298.